Neurochemical and functional interactions for improved perceptual decisions through training

Ke Jia*[1], Polytimi Frangou*[1], Vasilis M Karlaftis*[1], Joseph J Ziminski*[1], Joseph Giorgio[1], Reuben Rideaux[1], Elisa Zamboni[1], Victoria Hodgson[1], Uzay Emir[2], Zoe Kourtzi[1]

[1]Department of Psychology, University of Cambridge, CB2 3EB, Cambridge UK

[2]Purdue University School of Health Sciences, West Lafayette, Indiana, USA,

*These authors contributed equally to this work

Corresponding author:

Zoe Kourtzi

Department of Psychology

University of Cambridge

Downing Street, CB2 3EB

Cambridge, UK

Email: zk240@cam.ac.uk

Keywords: perceptual decisions, learning, MR spectroscopy, functional connectivity, transcranial direct current stimulation

Abstract

Learning and experience are known to improve our ability to make perceptual decisions. Yet, our understanding of the brain mechanisms that support improved perceptual decisions through training remains limited. Here, we test the neurochemical and functional interactions that support learning for perceptual decisions in the context of an orientation identification task. Using magnetic resonance spectroscopy (MRS), we measure neurotransmitters that are known to be involved in visual processing and learning (i.e. glutamate, GABA) in sensory (early visual cortex: EV) and decision-related (dorsolateral prefrontal cortex: DLPFC) brain regions. Using resting-state functional magnetic resonance imaging (rs-fMRI), we test for functional interactions between these regions that relate to decision processes. We demonstrate that training improves perceptual judgments (i.e. orientation identification) as indicated by faster rates of evidence accumulation after training. These learning-dependent changes in decision processes relate to lower EV glutamate levels and EV-DLPFC connectivity, suggesting that glutamatergic excitation and functional interactions between visual and dorsolateral prefrontal cortex facilitate perceptual decisions. Further, anodal transcranial direct current stimulation (tDCS) in early visual cortex impairs learning, suggesting a direct link between visual cortex excitation and perceptual decisions. Our findings advance our understanding of the role of learning in perceptual decision making, suggesting that glutamatergic excitation for efficient sensory processing and functional interactions between sensory and decision-related regions support improved perceptual decisions.

News and Noteworthy: Combining multimodal brain imaging (MRS-GABA, functional connectivity) with interventions (tDCs) we demonstrate that glutamatergic excitation and functional interactions between sensory (visual) and decision-related areas (dorsolateral prefrontal cortex) support our ability to optimize perceptual decisions through training.

Introduction

Making successful perceptual judgments entails integrating multiple sources of sensory information over time (Gold and Shadlen, 2007; Heekeren et al., 2008). For example, when deciding whether we have spotted a friend in the crowd, we accumulate information over time (e.g., as they approach, their appearance, clothing, and gait become clearer) and take into account not only the immediate sensory input but also our previous experience and knowledge (e.g. the likelihood of them appearing there and then).

Computational investigations have advanced our understanding of perceptual decision making by using sequential sampling models to decompose behavioral responses into decision processes (Bogacz et al. 2006; Ratcliff and McKoon 2008). In these sequential sampling models, participants accumulate evidence for two alternative choices and make their response when a critical amount of information (i.e. decision threshold) has been obtained in favor of one choice over the other. Previous work has implicated a network of regions in evidence accumulation for perceptual decision making, including parietal (Shadlen and Newsome 2001), frontal (Ding and Gold 2012), prefrontal (Heekeren et al. 2006; Philiastides et al. 2011) and ventral premotor cortex (Romo et al. 2004).

Further, previous behavioral (Dosher et al. 2013; Liu and Watanabe 2012; Petrov et al. 2011) and neuroimaging (Diaz et al. 2017; Jia et al. 2018; Kahnt et al. 2011) studies have proposed a role of learning in perceptual decision making, showing that training enhances evidence accumulation for perceptual judgments (e.g. discrimination of visual features) (Dutilh et al. 2009; Jia et al. 2018; Liu and Watanabe 2012; Petrov and Van Horn 2012; Zhang and Rowe 2014). Yet, our understanding of the brain mechanisms that alter decision processes through training remains limited.

Here, we interrogate the neurochemical and functional brain mechanisms that support our ability to improve our perceptual decisions due to training. We focus on perceptual learning, that is our ability to improve our perceptual judgements with training. We used an orientation identification task that involves identifying the orientation of a Gabor grating from Gaussian noise (Lu and Dosher 2009). We modelled behavioral performance using the drift diffusion model (i.e., a widely used sequential sampling model) (Bogacz et al. 2006; Ratcliff and McKoon 2008) to identify the decision processes involved in orientation identification and test the effect of training on these processes, rather than overall task performance.

Visual perceptual learning has been shown to engage a network of visual regions involved in sensory processing and frontoparietal regions involved in decision making (for reviews see Maniglia & Seitz, 2018; Vogels, 2010). In particular, training has been shown to alter processing in both visual cortex (Gilbert and Sigman 2007; Ito et al. 1998; Schoups et al. 2001; Sigman et al. 2005), and higher frontoparietal areas (Jia et al. 2018; Kahnt et al. 2011; Law and Gold 2010). Here we focus on early visual cortex and the dorsolateral prefrontal cortex that is known to be functionally connected to early visual cortex (Baker et al. 2018) and involved in perceptual decision making (Heekeren et al. 2006; Philiastides et al. 2011).

Further, previous studies have investigated the role of excitatory (glutamate: Glu) and inhibitory (γ-aminobutyric acid: GABA) neurotransmitters in visual processing and learning. Thanks to recent advances in MRS, it is now possible to reliably measure these neurotransmitters non-invasively in the human brain. MRS studies have shown that glutamatergic excitation, that is known to play a key role in long-term potentiation induction and plasticity (for a review see Valtcheva and Venance, 2019), relates to visual cortex activation (Ip et al. 2017; Lin et al. 2012), contrast sensitivity (Ip et al., 2019), motion discrimination (Schallmo et al. 2019) and object recognition (Lally et al. 2014). GABAergic inhibition in the visual cortex, as measured by MRS, has been implicated in orientation discrimination tasks (Edden et al. 2009; Rokem et al. 2011; Song et al. 2017) and visual perceptual learning (Frangou et al. 2018, 2019; Shibata et al. 2017). Further, the neurochemical balance between excitation and inhibition has been suggested to play a key role in brain-wide network interactions (Mann and Paulsen 2007). Human MRS studies have linked Glu and GABA concentrations at rest with functional connectivity as measured by rs-fMRI (Bachtiar et al. 2015; Duncan et al. 2013; Kapogiannis et al. 2013; Wang et al. 2020), consistent with the role of glutamatergic excitation and GABAergic inhibition in neural dynamics.

Here, we ask whether neurochemical processing within visual and decision-related areas and functional interactions between these regions relate to improved perceptual decisions due to training. Using MRS to measure neurotransmitter levels at rest, we test whether Glu and GABA+ levels in EV and DLPFC relate to learning-dependent changes in decision processes. Using rs-fMRI, we test whether functional connectivity between these regions relates to glutamatergic excitation or GABAergic inhibition and learning-dependent changes in decision processes. Our results demonstrate that training on an orientation identification task enhances information accumulation (i.e., improved drift rate). This behavioral improvement relates to lower EV glutamatergic excitation and functional connectivity between EV and DLPFC, suggesting that local excitatory processing in visual cortex and interactions between visual and decision-related areas contribute to optimizing perceptual decisions through training. Moving beyond correlational evidence, we use tDCS to perturb cortical excitability during training on the orientation identification task. Our results show that increasing excitation with anodal stimulation of the early visual cortex impairs learning in the orientation identification task, suggesting that low levels of excitation in the visual cortex are directly linked to efficient sensory processing for improved perceptual decisions.

Materials and Methods

Participants

Twenty-five participants (12 female; mean age 24 ± 3.7 years) took part in the main study and forty participants (13 female, age 21 ± 2.3 years) took part in the tDCS experiment (20 in the Anodal and 20 in the Sham group). All participants were right-handed, had normal or corrected-to-normal vision, did not receive any prescription medication, and gave written informed consent. The study was approved by the University of Cambridge Research Ethics committee [PRE.2017.57].

Experimental Design

Participants in the main study took part in one behavioral session in the lab and two brain imaging scans (before behavioral training) comprising rs-fMRI and MRS. Participants in the tDCS study took part in one behavioral session with stimulation in the lab.

Stimuli and Task

Experiments were controlled using MATLAB and Psychophysics toolbox 3.0 (Brainard 1997; Pelli 1997). For the behavioral session, stimuli were presented on a 21-inch CRT monitor (1600 × 1200 pixel resolution, 60 Hz frame rate) with Gamma correction at a distance of 50 cm. Stimuli comprised oriented Gabor patches that were presented against a uniform gray background. Gabor patches of random phase had a fixed diameter of 12°, SD of the Gaussian envelope of 2°, contrast of 0.03, and spatial frequency of 1 cycle/degree. Gaussian-distributed noise patterns had a contrast of 0.2. This contrast value was defined based on a pilot study that showed 60% accuracy in orientation identification before training. An independent assessor to the researchers who ran the experiments monitored the pre-training performance during data collection. The first set of 8 participants of the Anodal group were tested on the same contrast level as participants in the main experiment (i.e.

0.03). However, they showed lower pre-training accuracy than the expected 60% (mean accuracy = 55.9%). Therefore, we increased the contrast of the stimuli to 0.035 for the remaining participants in the tDCS experiment (12 for Anodal, 20 for Sham). Statistical analyses with and without the participants who performed the task with lower contrast showed similar results.

We tested participants on an orientation identification task (Figure 1a) during a test block (100 trials; no feedback) followed by five training blocks (100 trials each; with per trial feedback). Each trial began with a fixation cross for a jittered duration between 300-600ms (in increments of 100ms) followed by the noise patterns and Gabor patches. Two Gabor frames (i.e., 33ms) were presented in between pairs of noise frames (i.e. four noise frames were presented before and after the Gabor frames) to ensure temporal integration of the Gabor and noise patterns (Lu and Dosher 2009). Participants were asked to fixate and judge the orientation (left vs. right) of the Gabor patch (45° or 135°; Figure 1a).

MRI data acquisition

We collected MRI data on a 3T Siemens PRISMA scanner (Wolfson Brain Imaging Unit, Cambridge) using a 32-channel head coil. We acquired T1-weighted structural data (MPRAGE; TR = 2s; TE = 2.98ms; number of slices = 176; voxel size = 1mm isotropic) and echo-planar imaging (EPI) data at rest (gradient echo-pulse sequences; TR = 0.727s; TE = 34.6ms; number of slices = 72; voxel size = 2mm isotropic; Multiband factor = 8; flip angle = 48º; number of volumes = 825; duration = 10m; whole brain coverage). EPI data comprised two runs (10 min per run), during which participants fixated on a cross in the middle of the screen.

We collected MRS data using a 32-channel head coil and a MEGA-PRESS sequence (Mescher et al. 1998): TE = 68ms, TR = 3000ms; 256 transients of 2048 data points were acquired in 13 min experiment time; a 14.28ms Gaussian editing pulse was applied at 1.9

(ON) and 7.5 (OFF) ppm; water unsuppressed 16 transients (Table S1, following consensus guidelines (Lin et al. 2021)). Water suppression was achieved using variable power with optimized relaxation delays and outer volume suppression. We conducted automated shimming followed by manual shimming. We acquired spectra from two MRS voxels (25 x 25 x 25 mm^3): in early visual cortex (EV voxel) and the left dorsolateral prefrontal cortex (DLPFC voxel; Figure 2a). We manually positioned the MRS voxels using anatomical landmarks on each participant's T1 scan, ensuring that voxel placement was consistent across participants. The EV voxel was placed medially in the occipital lobe with the lower face aligned with the cerebellar tentorium and as posterior as possible towards the occipital pole given the voxel dimensions. The DLPFC voxel was placed within the left hemisphere and above the superior margin of the lateral ventricles. The center of gravity for the EV voxel was: x=0.8±1.8mm, y=-80.2±2.4mm, z=8.2±2.9mm in MNI space (partially covering V1 and V2 regions), and for the DLPFC voxel was: x=-24.4±2.0mm, y=33.0±7.0mm, z=25.1±6.2mm in MNI space. The order of the voxels was counterbalanced across participants. During the MRS acquisitions participants fixated on a cross in the middle of the screen to encourage similar levels of alertness across participants.

tDCS data acquisition

We used a multi-channel transcranial electrical stimulator (neuroConn DC-STIMULATOR MC, Ilmenau, Germany) to deliver anodal or sham stimulation in a double-blind manner. We used a pair of rubber electrodes (3×3 cm^2 stimulating electrode, 5×5 cm^2 reference electrode), placed in square sponges that had soaked in saline. For anodal stimulation, 1mA current was ramped up over 10s, was held at 1mA for the duration of training (~25min) and was subsequently ramped down over 10s. For sham stimulation, the current ramped up (10s) and down (10s) in the beginning of the session. To achieve consistent electrode placement across participants when targeting the early visual cortex, we used a 10–20 system EEG cap as reference and centered the anode on Oz and the cathode on Cz. This montage has been extensively used in tDCS studies targeting the early visual cortex (e.g. (Raveendran et al. 2020; Spiegel et al. 2013) and has been shown to successfully increase excitability in this region (Antal and Paulus 2008).

Data analysis

Behavioral data analysis

Three participants from the main study and one from the tDCS experiment (from the Sham group) were excluded due to high starting performance (over 75%). We further excluded 7 participants from the tDCS experiment (2 from the Anodal and 5 from the Sham group) due to atypical response times (i.e. RT<0.2s) that suggested the participants did not engage with the task. This resulted in N=22 for the main study and N=32 for the tDCS experiment (N=18 for Anodal, N=14 for Sham), consistent with sample sizes in our previous studies (Frangou et al. 2018). Following previous studies using a single-training session (Frangou et al. 2019) we calculated performance accuracy per participant and compared accuracy in the pre-training block to accuracy in the max-training block (i.e. we selected the block with the higher accuracy between the last two training blocks per participant to account for potential fatigue effects towards the end of the training).

Further, to model processes related to decision making, we fitted the behavioral data for each block using the Diffusion Model Analysis Toolbox (DMAT; Vandekerckhove and Tuerlinckx, 2008, 2007). The drift diffusion model (DDM) consisted of seven parameters: (1) The mean drift rate (DR) and (2) across-trial variability (s) in drift rate indicate stimulus discriminability; that is, a higher drift rate denotes faster and more accurate responses. The drift rate varies from trial to trial, following a normal distribution with mean DR and standard deviation s. (3) The decision threshold (TH) controls the speed-accuracy tradeoff and represents the amount of evidence required for making a decision. A higher decision threshold denotes slower but more accurate responses, suggesting that participants tend to make more cautious decisions. (4) The mean starting point (z), and (5) variability of starting point (sz) reflect the observer's prior bias at stimulus onset. In the case of the diffusion model, the starting point of the decision process at stimulus onset is assumed to vary randomly from trial-to-trial, according to a uniform distribution with mean z and standard deviation sz. This random variation may reflect, for example, the influence of recent preceding trials. (6) The mean non-decision time (Ter) and (7) variability of non-decision time (st) denote the time that includes early encoding processes (i.e. before the diffusion decision process) and late motor response processes (i.e. after the diffusion decision process). The non-decision time is assumed to vary randomly across trials according to a uniform distribution with mean Ter and standard deviation st. The diffusion model assumes that the observed response time is the sum of the non-decision component and the diffusion decision component.

Based on previous studies (Liu and Watanabe 2012; Petrov et al. 2011), we constructed five different models. Model 1 assumed that learning did not change any parameter of the model (Null model); Model 2 assumed that learning changed drift rate (DR model); Model 3 assumed that learning changed drift rate and decision threshold (DR-TH model); Model 4 assumed that learning changed drift rate, decision threshold and non-decision time (DR-TH-Ter model); Model 5 assumed that learning changed all the parameters of the model (Full model). We used Bayesian information criterion (BIC) for the five constructed models and selected model DR-TH-Ter that had the lowest mean BIC value across participants (i.e. null model: 3246.22, DR model: 3267.02, DR-TH model: 3234.13, DR-TH-Ter model: 3228.73, full model: 3308.36). Quantile-probability plots were used to inspect the model fitting. Data from one participant in the tDCS study (from the Anodal group) were excluded from further analysis as the model fit did not converge.

MRS data analysis

We pre-processed the MRS data using MRspa v1.5c (www.cmrr.umn.edu/downloads/mrspa/). We applied Eddy current, frequency and phase correction before subtracting the average ON and OFF spectra, resulting in edited spectra. We used LCModel (Provencher 2001) to quantify metabolite concentrations by fitting model spectra of glutamate (Glu), glutamine (Gln), γ-amino-butyric acid (GABA), glutathione (GSH) and N acetylaspartate (NAA) to the edited spectra (Figure 2a). The model spectra of all metabolites were generated based on previously reported chemical shifts and coupling constants using the GAMMA/PyGAMMA simulation library of VESPA (Versatile Simulation, Pulses and Analysis, (Soher et al. 2011)) for carrying out the density matrix formalism. A 20 x 20 spatial matrix was used to simulate the spatial variations inside and outside the nominal PRESS dimensions. Simulations were performed with the same RF pulses and sequence timings used on our 3T scanner.

We focused on glutamate rather than glutamine, as it is the primary excitatory neurotransmitter and it is known to play a key role in brain plasticity and learning (Riedel 2003). Glu has been shown to be separable from glutamine and reliably quantified when measured with MEGA-PRESS at 3T (Sanaei Nezhad et al. 2018) and the spectra are fitted using LCModel (O'Gorman et al. 2011; van Veenendaal et al. 2018). Our glutamate measurements are in agreement with the spectral quality criteria outlined in previous work (Sanaei Nezhad et al. 2018). Following these criteria, we were able to distinguish glutamate from glutamine for most participants. We conducted additional control analyses, excluding data in cases that Gln could not be fit (n=4, EV voxel).

We refer to GABA concentration as GABA+, as MRS measurements of GABA with MEGA-PRESS include co-edited macromolecules (Mullins et al. 2014). We referenced Glu and GABA+ concentrations to the concentration of water and validated our findings by referencing Glu and GABA+ to NAA to ensure our results were not driven by the chosen reference (Lunghi et al. 2015).

All spectra had linewidth below 10Hz and Glu and GABA+ Cramer-Rao lower bound (CRLB) values smaller than 10%. DLPFC data for 5 participants were excluded due to lipid contamination, as detected by visual inspection by two independent reviewers (PF, JZ), resulting in N=22 for EV and N=17 for DLPFC. Signal-to-noise ratio (SNR) was computed using LCModel as the amplitude of the NAA peak in the difference-spectrum divided by twice the root mean square of the residual signal (Provencher 2001). We report average concentrations of Glu and GABA+, in addition to quality indices (CRLB, linewidth, SNR), per MRS voxel (Table S2). To control for potential differences in data quality across participants, we performed control analyses that accounted for variability in absolute CRLB (Kreis 2016), linewidth and SNR across participants.

Further, we conducted whole brain tissue-type segmentation of the T1-weighted structural scan and calculated the percentage of gray matter (GM), white matter (WM) and cerebrospinal fluid (CSF) voxels in each MRS voxel. We then divided the Glu and GABA+ concentrations by [1-CSF fraction] to ensure our results were not driven by variability in tissue composition within the MRS voxel across participants and used these tissue-corrected values in further analyses.

rs-fMRI data pre-processing

We pre-processed the rs-fMRI data in SPM12.3 (v6906; www.fil.ion.ucl.ac.uk/spm/software/spm12/) following the Human Connectome Project (HCP) pipeline for multi-band data (Smith et al. 2013). In particular, we first coregistered (non-linear) the T1w structural images (after brain extraction) to MNI space to ensure that all participant data were in the same stereotactic space for statistical analysis. We then (a) corrected the EPI data for any spatial misalignments between EPI volumes due to head movement (i.e. aligned each run to its single band reference image), (b) coregistered the second EPI run to the first run (rigid body) to correct any spatial misalignments between runs, (c) coregistered the first EPI run to the structural image (rigid body) and (d) normalized them to MNI space for subsequent statistical analyses (applying the deformation field of the structural images). Data were only resliced after MNI normalization to minimize the number of interpolation steps. Following MNI normalization, (e) data were skull-stripped, (f) spatially smoothed with a 4mm Gaussian kernel to improve the signal-to-noise ratio and the alignment between participant data (two times the voxel size; (Chen and Calhoun 2018)), (g) wavelet despiked to remove any secondary motion artifacts (Patel et al. 2014), and (h) had linear drifts removed (linear detrending due to scanner noise). Slice-timing correction was not applied, following previous work on fast TR (sub-second) acquisition protocols (Smith et al. 2013). Data from 4 participants were excluded from further analysis due to head movement-related artifacts during the rs-fMRI acquisition, as measured by wavelet despiking (spike percentage higher than 10% (Patel et al. 2014)), resulting in a total of N=18.

Next, we applied spatial group Independent Component Analysis (ICA) using the Group ICA fMRI Toolbox (GIFT v3.0b) (http://mialab.mrn.org/software/gift/) to identify and remove components of noise. Principal Component Analysis was applied for dimensionality reduction, first at the subject level, then at the group level. The Minimum Description Length criteria (Rissanen 1978) were used to estimate the dimensionality and determine the number of independent components, resulting in 34 independent components. The ICA estimation (Infomax) was run 20 times and the component stability was estimated using ICASSO (Himberg et al. 2004). Following recent work on back-reconstruction methods for ICA denoising at the group level (Du et al. 2016), we used Group Information Guided ICA (GIG-ICA) back-reconstruction to reconstruct subject-specific components from the group components. We visually inspected the results and identified noise components according to published procedures (Griffanti et al. 2017). Using consensus voting among 3 experts (VK, PF, JG), we labelled 11 of the 34 components as noise that captured signal from veins, arteries, CSF pulsation, susceptibility and multi-band artefacts.

To clean the fMRI signals from motion artefacts and the noise components, we followed a soft cleanup ICA denoise approach (Griffanti et al. 2014). That is, we first regressed out the motion parameters (translation, rotation and their squares and derivatives; (Friston et al. 1996) from each voxel and ICA component time course. Second, we estimated the contribution of every ICA component to each voxel's time course (multiple regression). Finally, we subtracted the unique contribution of the noise components from each voxel's time course to avoid removing any shared signal between neuronal and noise components. We did not include the global signal as a nuisance regressor, as it has been shown to capture behaviorally relevant information (Li et al. 2019) and neuronal signals (for review see Uddin 2020). Following ICA denoise, the data were high-pass filtered at 0.01Hz and treated for serial correlations using the FAST autoregressive model (Corbin et al. 2018; Olszowy et al. 2019) and the residual time course from this step was used for all subsequent connectivity analyses.

Functional connectivity analysis

We computed functional connectivity between the two MRS voxels. First, we computed the overlap across participant MRS voxels for EV and DLPFC separately and created group MRS masks that included voxels present in at least 50% of the participants' MRS voxels. Then, for each participant and ROI, we computed the first eigenvariate across all gray matter voxels within the ROI to derive a single representative time course per ROI.

We computed the functional connectivity between the EV and the DLPFC MRS voxels as the Pearson correlation between the eigenvariate time course from each of the MRS masks. We then applied Fisher z-transform to the correlation coefficient and averaged across runs to derive an EV-DLPFC connectivity value per participant. To test for specificity of the

EV-DLPFC connectivity results, we computed the functional connectivity between EV and a control area (primary motor cortex: M1). We defined a left M1 mask of equal size to the MRS masks based on anatomical coordinates (MNI coordinates [-36, -26, 48]).

Statistical analysis

To test for within-subject differences across measurements, we conducted a repeated measures ANOVA in SPSS. For post-hoc pairwise comparisons we tested for significance at p=0.025 (Bonferroni corrected for two statistical tests). For testing the relationship of two or more variables, we used robust least-squares regression (*robustfit* function in MATLAB) for reweighting potential outliers. In particular, we used multiple regression models with two independent variables (DR and TH, or Glu and GABA+) to minimize the number of statistical tests. Prior to performing a multiple regression, we ensured that the independent variables are not collinear. For all control analyses, we used a simple linear regression model with the variable of interest (i.e. the variable that showed a significant relationship) and test for significant differences between predictors. For easier interpretation of the results, we also report a standardized r-coefficient by converting the regression's t-statistic with the following formula: $r = sign(t) * \sqrt{\frac{t^2}{t^2+df}}$. For visualization purposes, we plot the fitted lines according to the following formula: $y_{1,2} = b_0 + b_{1,2} * x_{1,2} + b_{2,1} * \mathrm{mean}(x_{2,1})$, where y_i is the expected outcome value for the i-th predictor, b_0 is the beta weight for the constant term, b_i is the weight for the i-th predictor, and x_i is the vector of the i-th predictor. In line with previous MRS studies (de la Fuente-Sandoval et al. 2016; Modinos et al. 2017) exploratory associations between additional functional connectivity measures (e.g. intrinsic connectivity) and our MRS and learning measures were assessed.

Results

Training alters perceptual decision processes

We tested participants on an orientation identification task during a pre-training test block (without feedback) and five training blocks (with per trial feedback) (Figure 1a). On each trial, participants were asked to identify the orientation (45° or 135°) of a Gabor grating that was masked with Gaussian noise. Our results showed that participants improved in their judgments within a single training session (Figure 1b), as indicated by significant differences in performance during training (repeated-measures ANOVA: main effect of block: $F(5,105)=3.04$, $p=0.013$). In particular, following previous studies (Frangou et al. 2019) using a single-training session, we compared performance (accuracy) in the pre-training block to maximum training performance (max-training; i.e., performance at the training block with the higher accuracy between the last two training blocks per participant). Our results showed significantly higher performance after training ($t(21)=4.43$, $p<0.001$), consistent with previous reports showing behavioral improvement for early learning (i.e., within a single training session; for a review see Sagi, 2011).

We next asked whether training alters processes related to decision making. We modelled the data with five different drift diffusion models following previous work (Liu and Watanabe 2012; Zhang and Rowe 2014). Using BIC as in previous studies (Liu and Watanabe 2012; Petrov et al. 2011), we selected the model with the lowest mean BIC value across participants. We then extracted the following parameters related to decision processes from this model (model 4: DR-TH-Ter Model): (1) drift rate (DR), indicating the rate at which participants accumulate information for making a perceptual judgment, (2) decision threshold (TH), indicating the amount of information required to make a judgment, and (3) non-decision time (Ter), indicating the time for early encoding processes and late motor response processes. Comparing the model parameters between pre-training and max-training blocks, we found that drift rate significantly increased after training ($t(21)=4.48$, $p<0.001$;

Figure 1c) and decision threshold significantly decreased after training (t(21)=-3.85, p=0.001; Figure 1d), whereas no significant changes were observed for the non-decision time due to training (t(21)=1.08, p=0.293). These results suggest that training improves the rate at which participants accumulate information and the amount of evidence they require for making a decision, rather than non-decision related processes.

Figure 1

Glutamate relates to evidence accumulation for perceptual decision making

Recent work has linked visual cortex glutamatergic excitation and GABAergic inhibition to perceptual judgments and learning (for a review see Ip and Bridge, 2021). Here, we tested the role of excitatory (Glu) and inhibitory (GABA) neurotransmitters in perceptual decision making processes, as identified by diffusion modeling of performance in the orientation identification task. We measured Glu and GABA+ at rest (i.e., participants had their eyes open and fixated on a central cross) from voxels placed in (a) the early visual cortex (EV MRS voxel; Figure 2a) that is known to be involved in orientation discrimination and learning (Jia et al. 2020; Schoups et al. 2001) and (b) the left dorsolateral prefrontal cortex (DLPFC MRS voxel; Figure 2a) that is known to be involved in the read-out of sensory information from visual cortex, transforming input to decision variables (Heekeren et al. 2004) and accumulating the decision variables during perceptual decision making (Heekeren et al. 2006; Philiastides et al. 2011). Further, previous studies have shown that activity in DLPFC correlates with drift rate (Heekeren et al. 2006) and disruption of processing in left DLPFC with brain stimulation impairs performance accuracy, corresponding to decreased drift rate (Philiastides et al. 2011). To test the link between these neurotransmitters and learning-dependent changes in decision processes due to training on the orientation identification task, we related Glu and GABA+ levels in these regions with change (i.e. max-training block minus pre-training block) in the drift diffusion model parameters that showed significant differences due to training (multiple regression with DR and TH as independent variables).

We found a significant negative relationship between EV Glu and DR change after training but not TH change (multiple regression: DR: $b=-2.13$, $t(19)=-2.83$, $r=-0.54$, $p=0.011$; TH: $b=-0.41$, $t(19)=-0.24$, $r=-0.05$, $p=0.815$; Figure 2b). The relationship of EV Glu with DR change was significantly different from the relationship of EV Glu with TH change ($Z=-2.05$, $p=0.041$; EV Glu – DR: $r=-0.59$; EV Glu – TH: $r=0.09$; DR – TH: $r=-0.36$), suggesting that EV Glu relates to DR rather than TH change. We didn't observe any significant relationship between: a) EV GABA+ and DR change nor TH change (multiple regression: DR: $b=-0.44$, $t(19)=-0.76$, $r=-0.17$, $p=0.458$; TH: $b=-1.83$, $t(19)=-1.37$, $r=-0.30$, $p=0.187$; Figure 2c), b) DLPFC Glu and DR change nor TH change (multiple regression: DR: $b=1.04$, $t(14)=1.17$, $r=0.30$, $p=0.262$; TH: $b=-4.46$, $t(14)=-1.10$, $r=-0.28$, $p=0.291$; Figure 2d), and c) DLPFC GABA+ and DR change nor TH change (multiple regression: DR: $b=-0.02$, $t(14)=-0.04$, $r=-0.01$, $p=0.969$; TH: $b=-3.17$, $t(14)=-1.54$, $r=-0.38$, $p=0.146$; Figure 2e). The relationship between EV Glu and DR change remained significant when we performed the following control analyses: a) referenced Glu to NAA rather than water ($b=-1.71$, $t(20)=-3.11$, $r=-0.57$, $p=0.006$), b) excluded 4 participants due to poor Gln fit ($b=-2.47$, $t(16)=-3.51$, $r=-0.66$, $p=0.003$), and c) controlled for MRS data quality (absolute CRLB: $b=-2.58$, $t(20)=-4.75$, $r=-0.73$, $p<0.001$; linewidth: $b=-1.78$, $t(20)=-3.00$, $r=-0.56$, $p=0.007$; SNR: $b=-2.27$, $t(20)=-3.97$, $r=-0.66$, $p=0.001$). Further, the relationship of EV Glu with DR change was significantly different from the relationship of EV GABA+ with DR change ($Z=-2.07$, $p=0.038$; EV Glu – DR: $r=-0.59$; EV GABA+ – DR: $r=-0.09$; EV Glu – GABA+: $r=0.26$), suggesting that EV Glu rather than GABA+ relate to information accumulation. There was no significant relationship between EV Glu and DR before training ($b=0.94$, $t(20)=1.01$, $r=0.22$, $p=0.324$), suggesting that our results could not be simply due to variability in pre-training performance. These results indicate a significant contribution of DR change to EV Glu, suggesting that faster rates of information accumulation after training relate to lower glutamatergic excitation in early visual cortex.

Figure 2

Visual-DLPFC functional connectivity for perceptual decision making

Previous work has shown that functional connectivity at rest predicts individual variability in a range of tasks (for reviews see Harmelech and Malach, 2013; Vaidya and Gordon, 2013), including perceptual learning (Baldassarre et al. 2012; Frangou et al. 2019). Further, previous studies have linked functional connectivity in visual and frontal cortex to perceptual judgments and learning-dependent plasticity (for reviews see Guerra-Carrillo et al., 2014; Kelly and Castellanos, 2014). Here, we tested whether functional interactions between early visual cortex and DLPFC—as measured by rs-fMRI—relate to decision making processes and neurochemical processing (glutamatergic, GABAergic) when training on an orientation identification task.

First, we tested whether functional connectivity between EV and DLPFC relates to drift rate and decision threshold (multiple regression with DR and TH as independent variables). We measured functional connectivity as the correlation between rs-fMRI time courses from gray matter voxels within the EV and DLPFC voxels (EV-DLPFC connectivity). We observed a significant negative relationship between EV-DLPFC functional connectivity and DR change but not TH change (multiple regression: DR; $b=-2.32$, $t(15)=-2.94$, $r=-0.60$, $p=0.010$; TH; $b=1.91$, $t(15)=0.63$, $r=0.16$, $p=0.538$; Figure 3a). The relationship of EV-DLPFC functional connectivity with DR change was significantly different from the relationship of EV-DLPFC functional connectivity with TH change ($Z=-2.03$, $p=0.043$; (EV-DLPFC connectivity – DR: $r=-0.60$; EV-DLPFC connectivity – TH: $r=0.07$; DR – TH: $r=-0.36$), suggesting that EV-DLPFC functional connectivity relates to DR rather than TH change. There was no significant relationship between EV-DLPFC functional connectivity and DR before training (b=0.59, t(16)=0.66, r=0.16, p=0.521), suggesting that our results could not be simply due to variability in pre-training performance. We did not observe a significant relationship of functional connectivity between early visual cortex and a control region (M1) with DR change (b=-1.57, t(16)=-1.64, r=-0.38, p=0.121), nor when controlling for the relationship with EV-DLPFC connectivity (b=0.41, t(16)=0.31, r=0.08, p=0.762), suggesting that our results are specific to EV-DLPFC connectivity. Thus, our results indicate a significant contribution of DR change to EV-DLPFC connectivity, suggesting that faster rates of information accumulation due to training relate to lower functional connectivity between early visual and dorsolateral prefrontal cortex.

Figure 3

Second, we tested whether EV-DLPFC functional connectivity relates to glutamatergic or GABAergic processing in EV and DLPFC (multiple regression with Glu and GABA+ as independent variables). We observed a significant positive relationship between EV-DLPFC connectivity and EV Glu but not EV GABA+ (multiple regression: EV Glu: b=0.34, t(15)=2.18, r=0.49, p=0.046; EV GABA+: b=0.61, t(15)=1.89, r=0.44, p=0.078; Figure 3b). The relationship of EV-DLPFC functional connectivity with EV Glu was not significantly different from that of EV-DLPFC functional connectivity with EV GABA+ (Z=0.22, p=0.824; (EV-DLPFC connectivity – EV Glu: r=0.53; EV-DLPFC connectivity – EV GABA+: r=0.48; EV Glu – EV GABA+: r=0.26). We didn't observe any significant relationships between EV-DLPFC and DLPFC Glu nor DLPFC GABA+ (multiple regression: DLPFC Glu: b=-0.19, t(12)=-0.64, r=-0.18, p=0.531; DLPFC GABA+: b=-0.14, t(12)=-0.22, r=-0.06, p=0.826; Figure 3c). The relationship between EV-DLPFC connectivity and EV Glu remained significant when we performed the following control analyses: a) referenced Glu to NAA rather than water (b=0.66, t(16)=2.88, r=0.58, p=0.011), b) excluded 4 participants due to poor Gln fit (b=0.51, t(13)=2.87, r=0.62, p=0.013), and c) controlled for

MRS data quality (absolute CRLB: b=0.55, t(16)=3.07, r=0.61, p=0.007; linewidth: b=0.42, t(16)=2.56, r=0.54, p=0.021; SNR: b=0.44, t(16)=2.74, r=0.57, p=0.015). Further, we found no significant relationship between EV-M1 functional connectivity and EV Glu (b=0.33, t(16)=1.72, r=0.40, p=0.104), nor when controlling for the relationship with EV-DLPFC connectivity (b=-0.08, t(16)=-0.33, r=-0.08, p=0.744), suggesting that our results are specific to EV-DLPFC connectivity. Thus, our results indicate a significant contribution of EV Glu to EV-DLPFC connectivity, suggesting that lower early visual cortex excitation relates to lower functional connectivity between early visual and dorsolateral prefrontal cortex to support faster rates of information accumulation.

Increasing excitation in the visual cortex impairs learning

To extend beyond correlational approaches, we employed anodal tDCS to perturb cortical excitability during training on the orientation identification task. Anodal tDCS is an excitatory stimulation protocol that has been shown to increase cortical excitability in visual (Antal et al. 2004) and motor cortex (Nitsche and Paulus 2000). We have previously shown that anodal tDCS results in improved learning in the context of a visual task that requires enhanced excitability (Frangou et al. 2018). As our main experiment showed that lower visual cortex excitation relates to faster drift rate after training on the orientation identification task, we hypothesized that excitatory stimulation would impair learning compared to sham stimulation.

To test this hypothesis, we trained two groups of participants on the orientation identification task, one receiving anodal and the other sham stimulation during training. As in the main experiment, we compared accuracy, DR and TH in the max-training block against the pre-training block. We found that participants who received anodal stimulation during training showed lower improvement after training compared to those who received sham stimulation. In particular, a repeated measures ANOVA on accuracy showed a significant

Group (Anodal, Sham) x Block (pre-training, max-training) interaction ($F(1,30)=4.68$, $p=0.039$; Figure 4a) and post-hoc comparisons showed significant performance improvement after training (i.e. increased accuracy) for the Sham ($t(13)=3.23$, $p=0.004$) but not the Anodal group ($t(17)=0.95$, $p=0.356$).

Further, a repeated measures ANOVA on DR showed a significant Group (Anodal, Sham) x Block (pre-training, max-training) interaction ($F(1,29)=8.39$, $p=0.007$; Figure 4b). Post-hoc comparisons showed significant changes in DR after training (i.e. faster drift rate) for the Sham ($t(13)=3.07$, $p=0.009$) but not the Anodal group ($t(16)=-0.001$, $p=0.999$), suggesting that participants in the Anodal group showed slower drift rate after training compared to those in the Sham group. Finally, a repeated measures ANOVA on TH showed a significant main effect of Block ($F(1,29)=10.59$, $p=0.003$; Figure 4c) but not a significant Group (Anodal, Sham) x Block (pre-training, max-training) interaction ($F(1,29)=0.88$, $p=0.356$), suggesting that the effect of the anodal stimulation was specific to the rate of information accumulation. Note that, DR before training was not different between the Anodal and Sham groups (Anodal vs. Sham: $t(29)=0.65$, $p=0.521$) and did not differ between the stimulation groups and the main study (one-way ANOVA with Group (Anodal, Sham, no-stimulation): $F(2,52)=0.57$, $p=0.571$), suggesting that the tDCS effects we observed after training were not due to variability across participants before training. We found similar results in a smaller group of participants (after removing six participants from the Anodal group who performed the task at a lower contrast level; see Methods); that is, repeated measures ANOVAs showed a significant Group x Block interaction for DR ($F(1,24)=5.20$, $p=0.032$, post-hoc for Anodal: $t(11)=1.09$, $p=0.301$) but not TH ($F(1,24)=0.27$, $p=0.610$).

Figure 4

Discussion

Training is known to improve perceptual decisions. Here, we test the neurochemical and functional connectivity mechanisms that support improved perceptual decisions due to training. Using MRS, we test for glutamatergic and GABAergic processing in early visual and decision-related regions. Using rs-fMRI, we test for functional interactions between these regions that relate to decision processes. Modelling behavioral performance using a drift diffusion model, we demonstrate that training results in faster evidence accumulation for orientation identification. These learning-dependent changes in decision processes relate to glutamate levels in visual cortex and functional connectivity between visual and dorsolateral prefrontal cortex. Our results suggest that efficient sensory processing and functional interactions between sensory and decision-related regions support improved decision making through training. Further, perturbing cortical excitability using tDCS disrupts evidence accumulation during training, providing a direct link between visual cortex excitation and perceptual decisions. Our findings advance our understanding of the role of learning in decision making in the following respects.

First, we show that training improves behavioral performance on a visual orientation identification task by increasing the information accumulation rate and reducing the information needed to make a judgment. This is consistent with previous studies showing that training facilitates information accumulation for perceptual decision making (Dutilh et al. 2009; Liu and Watanabe 2012; Petrov et al. 2011; Zhang and Rowe 2014). Further, our results using single-session training are consistent with previous work showing learning-dependent changes early in the training (Frangou et al. 2018, 2019; Karni and Sagi 1993).

Second, we demonstrate that glutamatergic excitation in the early visual cortex relates to early learning-dependent changes in sensory information processing during the decision processes (Jia et al. 2018; Ratcliff and McKoon 2008). Our results show that lower resting levels of early visual cortex glutamate, rather than GABA+, relate to increased drift rate after training, suggesting that lower excitatory processing in visual cortex relates to faster information accumulation after training. This relationship is shown to be specific to glutamatergic rather than GABAergic processing in visual cortex. While it remains debated whether MRS measures synaptic vs. extra-synaptic neurotransmitter concentration (Stagg 2014), some previous studies have linked glutamatergic excitation to visual discriminations (e.g. (Ip et al. 2019; Lally et al. 2014; Schallmo et al. 2019), while others GABAergic inhibition to performance in visual tasks (Edden et al. 2009; Frangou et al. 2018, 2019; Karlaftis et al. 2021; Rideaux and Welchman 2018; Shibata et al. 2017). Our results provide evidence that cortical glutamatergic excitation, known to relate to gain control mechanisms (Katzner et al. 2011), is involved in information accumulation during decision making.

Previous studies have implicated frontoparietal networks in information accumulation during visual tasks (FitzGerald et al. 2015; Mazurek et al. 2003; Pisauro et al. 2017); yet, recent evidence suggests that stimulus (rather than value) information accumulation engages visual areas (Krueger et al. 2017). Our results highlight a key role for early visual cortex in decision making processes, showing that glutamate in early visual cortex (as measured by MRS at rest) relates to increased accumulation of information after training. This relationship was not significant for drift rate before training, suggesting a link between excitatory processing in visual cortex and improved perceptual decisions after training. It is possible that optimizing information accumulation with training relates to more efficient input processing in the visual cortex that involves reduced excitatory processing. This interpretation is consistent with previous studies showing that lower fMRI BOLD in decision-related areas relates to shorter duration of information accumulation (Pisauro et al. 2017).

Further, it is possible, that in the presence of external noise, training reduces activity in visual cortex, as reflected by lower levels of glutamatergic excitability and reduced learning under excitatory stimulation. These reduced levels of excitation may correspond to exclusion of external noise (Lu et al. 2011), resulting in improved behavioral performance at early stages of learning (i.e. single training protocol employed in our study). The lack of a significant relationship between DLPFC MRS measures and learning may suggest that learning— at early stages of training (i.e., single training session)— alters stimulus processing (i.e., sensory processes) in early visual cortex, rather than information accumulation processes in DLPFC. These results are consistent with the reverse hierarchy theory of perceptual learning, suggesting that training on difficult tasks (as in the case of the task employed in our study) engages early visual cortex (Ahissar and Hochstein 2004).

Extending beyond correlational approaches, our tDCS intervention provides evidence for a direct link between excitatory processing in visual cortex and perceptual decisions, showing that increasing levels of excitation in the visual cortex through anodal tDCS disrupts information accumulation during training. At first glance, our results appear to be in contrast to previous studies showing that anodal tDCS facilitates performance in visual perception and memory tasks that involve excitatory processing (Barron et al. 2016; Frangou et al. 2018). Yet, the disruption of learning we observed due to anodal tDCS is in agreement with the negative relationship between visual cortex excitation and rate of information accumulation in the context of our orientation identification task. Interestingly, previous work using transcranial random noise stimulation (tRNS) during training on a fine orientation discrimination task has shown that tRNS improves performance compared to anodal or sham tDCS (Fertonani et al. 2011; Pirulli et al. 2013). While its mechanism of action remains debated, it is proposed that tRNS boosts signal detection by introducing stochastic resonance and enhancing processing of subthreshold stimuli (van der Groen and Wenderoth 2016). As low-contrast signal detection (van der Groen and Wenderoth 2016) and information accumulation in a perceptual decision making task (van der Groen et al. 2018) have been shown to benefit from tRNS, it would be interesting to test in future studies whether tRNS stimulation improves orientation identification performance.

Third, we demonstrate that functional connectivity between visual and decision-related regions relates to learning-dependent changes in decision making processes and glutamatergic processing in visual cortex. In particular, our results show that lower visual-frontal connectivity relates to faster information accumulation due to training and lower excitatory input processing, as indicated by lower levels of glutamate in visual cortex. It is possible that faster information accumulation due to training relates to more efficient local processing in visual cortex and interactions between visual and decision-related regions. This is consistent with previous work implicating local gain control mechanisms in visual cortex and reduced inter-areal connectivity when learning to identify targets in noise (Frangou et al. 2019). Further, our findings highlight the role of neurochemical mechanisms in network connectivity, consistent with previous studies showing a link between glutamate levels and functional connectivity at rest within and between brain (Duncan et al. 2013; Kapogiannis et al. 2013).

In sum, our findings provide novel insights in understanding the neurochemical mechanisms that underlie perceptual decision making. Combining multimodal brain imaging (MRS, rs-fMRI) with brain stimulation and computational modeling reveals a key role of glutamatergic processing for perceptual decisions. Our findings demonstrate that efficient local processing related to glutamatergic excitation and inter-areal connectivity supports improved perceptual decisions through training. In this work, we focused on measurements of neurotransmitters and connectivity at rest. Future work combining tDCS with multi-modal brain imaging during training could investigate functional changes in neurotransmission to uncover its role in regulating network activity and connectivity for learning and brain plasticity.

Acknowledgements

We would like to thank Daniel Martin and Oliver Vij for help with data collection; the MR physics and radiographer teams at the Wolfson Brain Imaging Unit and the Cognition and Brain Sciences Unit for their support and help with data collection. All authors declare that they have no conflict of interest.

Funding

This work was supported by grants to ZK from the Biotechnology and Biological Sciences Research Council [grant numbers H012508, BB/P021255/1], the Wellcome Trust [grant number 205067/Z/16/Z], the European Community's Seventh Framework Programme (FP7/2007-2013) under agreement PITN-GA-2011-290011, and to KJ from the European Union's Horizon 2020 research and innovation programme under grant agreements No 840271.

References

Ahissar M, **Hochstein S**. The reverse hierarchy theory of visual perceptual learning. *Trends Cogn Sci* 8: 457–464, 2004.

Antal A, **Kincses TZ**, **Nitsche MA**, **Bartfai O**, **Paulus W**. Excitability Changes Induced in the Human Primary Visual Cortex by Transcranial Direct Current Stimulation: Direct Electrophysiological Evidence. *Investig Opthalmology Vis Sci* 45: 702, 2004.

Antal A, **Paulus W**. Transcranial Direct Current Stimulation and Visual Perception. *Perception* 37: 367–374, 2008.

Bachtiar V, **Near J**, **Johansen-Berg H**, **Stagg CJ**. Modulation of GABA and resting state functional connectivity by transcranial direct current stimulation. *Elife* 4: 1–9, 2015.

Baker CM, **Burks JD**, **Briggs RG**, **Conner AK**, **Glenn CA**, **Morgan JP**, **Stafford J**, **Sali G**, **McCoy TM**, **Battiste JD**, **O'Donoghue DL**, **Sughrue ME**. A Connectomic Atlas of the Human Cerebrum—Chapter 2: The Lateral Frontal Lobe. *Oper Neurosurg* 15: S10–S74, 2018.

Baldassarre A, **Lewis CM**, **Committeri G**, **Snyder AZ**, **Romani GL**, **Corbetta M**. Individual variability in functional connectivity predicts performance of a perceptual task. *Proc Natl Acad Sci* 109: 3516–3521, 2012.

Barron HC, **Vogels TP**, **Emir UE**, **Makin TR**, **O'Shea J**, **Clare S**, **Jbabdi S**, **Dolan RJ**, **Behrens TEJ**. Unmasking Latent Inhibitory Connections in Human Cortex to Reveal Dormant Cortical Memories. *Neuron* 90: 191–203, 2016.

Bogacz R, **Brown E**, **Moehlis J**, **Holmes P**, **Cohen JD**. The physics of optimal decision making: A formal analysis of models of performance in two-alternative forced-choice tasks. *Psychol Rev* 113: 700–765, 2006.

Brainard DH. The Psychophysics Toolbox. [Online]. *Spat Vis* 10: 433–6, 1997http://www.ncbi.nlm.nih.gov/pubmed/9176952.

Chen Z, **Calhoun V**. Effect of Spatial Smoothing on Task fMRI ICA and Functional

Connectivity. *Front Neurosci* 12: 15, 2018.

Corbin N, **Todd N**, **Friston KJ**, **Callaghan MF**. Accurate modeling of temporal correlations in rapidly sampled fMRI time series. *Hum Brain Mapp* 39: 3884–3897, 2018.

Diaz JA, **Queirazza F**, **Philiastides MG**. Perceptual learning alters post-sensory processing in human decision-making. *Nat Hum Behav* 1: 0035, 2017.

Ding L, **Gold JI**. Neural Correlates of Perceptual Decision Making before, during, and after Decision Commitment in Monkey Frontal Eye Field. *Cereb Cortex* 22: 1052–1067, 2012.

Dosher BA, **Jeter P**, **Liu J**, **Lu Z-L**. An integrated reweighting theory of perceptual learning. *Proc Natl Acad Sci* 110: 13678–13683, 2013.

Du Y, **Allen EA**, **He H**, **Sui J**, **Wu L**, **Calhoun VD**. Artifact removal in the context of group ICA: A comparison of single-subject and group approaches. *Hum Brain Mapp* 37: 1005–1025, 2016.

Duncan NW, **Wiebking C**, **Tiret B**, **Marjańska M**, **Hayes DJ**, **Lyttleton O**, **Doyon J**, **Northoff G**. Glutamate Concentration in the Medial Prefrontal Cortex Predicts Resting-State Cortical-Subcortical Functional Connectivity in Humans. *PLoS One* 8: e60312, 2013.

Dutilh G, **Vandekerckhove J**, **Tuerlinckx F**, **Wagenmakers E-J**. A diffusion model decomposition of the practice effect. *Psychon Bull Rev* 16: 1026–1036, 2009.

Edden RAE, **Muthukumaraswamy SD**, **Freeman TCA**, **Singh KD**. Orientation Discrimination Performance Is Predicted by GABA Concentration and Gamma Oscillation Frequency in Human Primary Visual Cortex. *J Neurosci* 29: 15721–15726, 2009.

Fertonani A, **Pirulli C**, **Miniussi C**. Random Noise Stimulation Improves Neuroplasticity in Perceptual Learning. *J Neurosci* 31: 15416–15423, 2011.

FitzGerald THB, **Moran RJ**, **Friston KJ**, **Dolan RJ**. Precision and neuronal dynamics in the human posterior parietal cortex during evidence accumulation. *Neuroimage* 107: 219–228, 2015.

Frangou P, **Correia M**, **Kourtzi Z**. GABA, not BOLD, reveals dissociable learning-dependent plasticity mechanisms in the human brain. *Elife* 7: 1–22, 2018.

Frangou P, **Emir UE**, **Karlaftis VM**, **Nettekoven C**, **Hinson EL**, **Larcombe S**, **Bridge H**, **Stagg CJ**, **Kourtzi Z**. Learning to optimize perceptual decisions through suppressive interactions in the human brain. *Nat Commun* 10: 474, 2019.

Friston KJ, **Williams S**, **Howard R**, **Frackowiak RSJJ**, **Turner R**. Movement-Related effects in fMRI time-series. *Magn Reson Med* 35: 346–355, 1996.

Gilbert CD, **Sigman M**. Brain States: Top-Down Influences in Sensory Processing. *Neuron* 54: 677–696, 2007.

Gold JI, **Shadlen MN**. The Neural Basis of Decision Making. *Annu Rev Neurosci* 30: 535–574, 2007.

Griffanti L, **Douaud G**, **Bijsterbosch J**, **Evangelisti S**, **Alfaro-Almagro F**, **Glasser MF**, **Duff EP**, **Fitzgibbon S**, **Westphal R**, **Carone D**, **Beckmann CF**, **Smith SM**. Hand classification of fMRI ICA noise components. *Neuroimage* 154: 188–205, 2017.

Griffanti L, **Salimi-Khorshidi G**, **Beckmann CF**, **Auerbach EJ**, **Douaud G**, **Sexton CE**, **Zsoldos E**, **Ebmeier KP**, **Filippini N**, **Mackay CE**, **Moeller S**, **Xu J**, **Yacoub E**, **Baselli G**, **Ugurbil K**, **Miller KL**, **Smith SM**. ICA-based artefact removal and accelerated fMRI acquisition for improved resting state network imaging. *Neuroimage* 95: 232–247, 2014.

van der Groen O, **Tang MF**, **Wenderoth N**, **Mattingley JB**. Stochastic resonance enhances the rate of evidence accumulation during combined brain stimulation and perceptual decision-making. *PLOS Comput Biol* 14: e1006301, 2018.

van der Groen O, **Wenderoth N**. Transcranial Random Noise Stimulation of Visual Cortex: Stochastic Resonance Enhances Central Mechanisms of Perception. *J Neurosci* 36: 5289–5298, 2016.

Guerra-Carrillo B, **Mackey AP**, **Bunge SA**. Resting-State fMRI: A Window into Human Brain Plasticity. *Neurosci* 20: 522–533, 2014.

Harmelech T, **Malach R**. Neurocognitive biases and the patterns of spontaneous correlations in the human cortex. *Trends Cogn Sci* 17: 606–615, 2013.

Heekeren HR, **Marrett S**, **Bandettini PA**, **Ungerleider LG**. A general mechanism for perceptual decision-making in the human brain. *Nature* 431: 859–862, 2004.

Heekeren HR, **Marrett S**, **Ruff DA**, **Bandettini PA**, **Ungerleider LG**. Involvement of human left dorsolateral prefrontal cortex in perceptual decision making is independent of response modality. *Proc Natl Acad Sci* 103: 10023–10028, 2006.

Heekeren HR, **Marrett S**, **Ungerleider LG**. The neural systems that mediate human perceptual decision making. *Nat Rev Neurosci* 9: 467–479, 2008.

Himberg J, **Hyvärinen A**, **Esposito F**. Validating the independent components of neuroimaging time series via clustering and visualization. *Neuroimage* 22: 1214–1222, 2004.

Ip IB, **Berrington A**, **Hess AT**, **Parker AJ**, **Emir UE**, **Bridge H**. Combined fMRI-MRS acquires simultaneous glutamate and BOLD-fMRI signals in the human brain. *Neuroimage* 155: 113–119, 2017.

Ip IB, **Bridge H**. Investigating the neurochemistry of the human visual system using magnetic resonance spectroscopy. *Brain Struct Funct* 1: 3, 2021.

Ip IB, **Emir UE**, **Parker AJ**, **Campbell J**, **Bridge H**. Comparison of Neurochemical and BOLD Signal Contrast Response Functions in the Human Visual Cortex. *J Neurosci* 39: 7968–7975, 2019.

Ito M, **Westheimer G**, **Gilbert CD**. Attention and Perceptual Learning Modulate Contextual Influences on Visual Perception. *Neuron* 20: 1191–1197, 1998.

Jia K, **Xue X**, **Lee J-H**, **Fang F**, **Zhang J**, **Li S**. Visual perceptual learning modulates decision network in the human brain: The evidence from psychophysics, modeling, and functional magnetic resonance imaging. *J Vis* 18: 9, 2018.

Jia K, **Zamboni E**, **Kemper V**, **Rua C**, **Goncalves NR**, **Ng AKT**, **Rodgers CT**, **Williams G**, **Goebel R**, **Kourtzi Z**. Recurrent Processing Drives Perceptual Plasticity. *Curr Biol* 30: 4177-4187.e4, 2020.

Kahnt T, **Grueschow M**, **Speck O**, **Haynes J-D**. Perceptual Learning and Decision-Making in Human Medial Frontal Cortex. *Neuron* 70: 549–559, 2011.

Kapogiannis D, **Reiter DA**, **Willette AA**, **Mattson MP**. Posteromedial cortex glutamate and GABA predict intrinsic functional connectivity of the default mode network. *Neuroimage* 64: 112–119, 2013.

Karlaftis VM, **Giorgio J**, **Zamboni E**, **Frangou P**, **Rideaux R**, **Ziminski JJ**, **Kourtzi Z**. Functional Interactions between Sensory and Memory Networks for Adaptive Behavior. *Cereb Cortex* 1–12, 2021.

Karni A, **Sagi D**. The time course of learning a visual skill. *Nature* 365: 250–252, 1993.

Katzner S, **Busse L**, **Carandini M**. GABAA Inhibition Controls Response Gain in Visual Cortex. *J Neurosci* 31: 5931–5941, 2011.

Kelly C, **Castellanos FX**. Strengthening Connections: Functional Connectivity and Brain Plasticity. *Neuropsychol Rev* 24: 63–76, 2014.

Kreis R. The trouble with quality filtering based on relative Cramér-Rao lower bounds. *Magn Reson Med* 75: 15–18, 2016.

Krueger PM, **van Vugt MK**, **Simen P**, **Nystrom L**, **Holmes P**, **Cohen JD**. Evidence accumulation detected in BOLD signal using slow perceptual decision making. *J Neurosci Methods* 281: 21–32, 2017.

de la Fuente-Sandoval C, **Reyes-Madrigal F**, **Mao X**, **León-Ortiz P**, **Rodríguez-Mayoral O**, **Solís-Vivanco R**, **Favila R**, **Graff-Guerrero A**, **Shungu DC**. Cortico-Striatal GABAergic and Glutamatergic Dysregulations in Subjects at Ultra-High Risk for Psychosis Investigated with Proton Magnetic Resonance Spectroscopy. *Int J Neuropsychopharmacol* 19: pyv105, 2016.

Lally N, **Mullins PG**, **Roberts M V.**, **Price D**, **Gruber T**, **Haenschel C**. Glutamatergic correlates of gamma-band oscillatory activity during cognition: A concurrent ER-MRS and EEG study. *Neuroimage* 85: 823–833, 2014.

Law CT, **Gold JI**. Shared mechanisms of perceptual learning and decision making. *Top Cogn Sci* 2: 226–238, 2010.

Li J, **Bolt T**, **Bzdok D**, **Nomi JS**, **Yeo BTT**, **Spreng RN**, **Uddin LQ**. Topography and behavioral relevance of the global signal in the human brain. *Sci Rep* 9: 14286, 2019.

Lin A, **Andronesi O**, **Bogner W**, **Choi I**, **Coello E**, **Cudalbu C**, **Juchem C**, **Kemp GJ**, **Kreis R**, **Krššák M**, **Lee P**, **Maudsley AA**, **Meyerspeer M**, **Mlynarik V**, **Near J**, **Öz G**, **Peek AL**, **Puts NA**, **Ratai E**, **Tkáč I**, **Mullins PG**. Minimum Reporting Standards for in vivo Magnetic Resonance Spectroscopy (MRSinMRS): Experts' consensus recommendations. *NMR Biomed* 34: e4484, 2021.

Lin Y, **Stephenson MC**, **Xin L**, **Napolitano A**, **Morris PG**. Investigating the Metabolic Changes due to Visual Stimulation using Functional Proton Magnetic Resonance Spectroscopy at 7 T. *J Cereb Blood Flow Metab* 32: 1484–1495, 2012.

Liu CC, **Watanabe T**. Accounting for speed- accuracy tradeoff in perceptual learning. *Vision Res* 61: 107–114, 2012.

Lu Z-L, **Dosher BA**. Mechanisms of perceptual learning. *Learn Percept* 1: 19–36, 2009.

Lu Z-L, **Li X**, **Tjan BS**, **Dosher BA**, **Chu W**. Attention Extracts Signal in External Noise: A BOLD fMRI Study. *J Cogn Neurosci* 23: 1148–1159, 2011.

Lunghi C, **Emir UE**, **Morrone MC**, **Bridge H**. Short-Term Monocular Deprivation Alters GABA in the Adult Human Visual Cortex. *Curr Biol* 25: 1496–1501, 2015.

Maniglia M, **Seitz AR**. Towards a whole brain model of Perceptual Learning. *Curr Opin Behav Sci* 20: 47–55, 2018.

Mann EO, **Paulsen O**. Role of GABAergic inhibition in hippocampal network oscillations. *Trends Neurosci* 30: 343–349, 2007.

Mazurek ME, **Roitman JD**, **Ditterich J**, **Shadlen MN**. A Role for Neural Integrators in Perceptual Decision Making. *Cereb Cortex* 13: 1257–1269, 2003.

Mescher M, **Merkle H**, **Kirsch J**, **Garwood M**, **Gruetter R**. Simultaneousin vivo spectral editing and water suppression. *NMR Biomed* 11: 266–272, 1998.

Modinos G, **McLaughlin A**, **Egerton A**, **McMullen K**, **Kumari V**, **Barker GJ**, **Keysers C**, **Williams SCR**. Corticolimbic hyper-response to emotion and glutamatergic function in people with high schizotypy: a multimodal fMRI-MRS study. *Transl Psychiatry* 7: e1083–e1083, 2017.

Mullins PG, **McGonigle DJ**, **O'Gorman RL**, **Puts NAJ**, **Vidyasagar R**, **Evans CJ**, **Edden RAE**. Current practice in the use of MEGA-PRESS spectroscopy for the detection of GABA. *Neuroimage* 86: 43–52, 2014.

Nitsche MA, **Paulus W**. Excitability changes induced in the human motor cortex by weak transcranial direct current stimulation. *J Physiol* 527: 633–639, 2000.

O'Gorman RL, **Michels L**, **Edden RA**, **Murdoch JB**, **Martin E**. In vivo detection of GABA and glutamate with MEGA-PRESS: Reproducibility and gender effects. *J Magn Reson Imaging* 33: 1262–1267, 2011.

Olszowy W, **Aston J**, **Rua C**, **Williams GB**. Accurate autocorrelation modeling substantially improves fMRI reliability. *Nat Commun* 10: 1220, 2019.

Patel AX, **Kundu P**, **Rubinov M**, **Jones PS**, **Vértes PE**, **Ersche KD**, **Suckling J**, **Bullmore ET**. A wavelet method for modeling and despiking motion artifacts from resting-state fMRI time series. *Neuroimage* 95: 287–304, 2014.

Pelli DG. The VideoToolbox software for visual psychophysics: transforming numbers into movies. *Spat Vis* 10: 437–442, 1997.

Petrov AA, **Van Horn NM**. Motion aftereffect duration is not changed by perceptual learning: Evidence against the representation modification hypothesis. *Vision Res* 61: 4–14, 2012.

Petrov AA, **Van Horn NM**, **Ratcliff R**. Dissociable perceptual-learning mechanisms revealed by diffusion-model analysis. *Psychon Bull Rev* 18: 490–497, 2011.

Philiastides MG, **Auksztulewicz R**, **Heekeren HR**, **Blankenburg F**. Causal Role of

Dorsolateral Prefrontal Cortex in Human Perceptual Decision Making. *Curr Biol* 21: 980–983, 2011.

Pirulli C, **Fertonani A**, **Miniussi C**. The Role of Timing in the Induction of Neuromodulation in Perceptual Learning by Transcranial Electric Stimulation. *Brain Stimul* 6: 683–689, 2013.

Pisauro MA, **Fouragnan E**, **Retzler C**, **Philiastides MG**. Neural correlates of evidence accumulation during value-based decisions revealed via simultaneous EEG-fMRI. *Nat Commun* 8: 15808, 2017.

Provencher SW. Automatic quantitation of localizedin vivo1H spectra with LCModel. *NMR Biomed* 14: 260–264, 2001.

Ratcliff R, **McKoon G**. The Diffusion Decision Model: Theory and Data for Two-Choice Decision Tasks. *Neural Comput* 20: 873–922, 2008.

Raveendran RN, **Tsang K**, **Tiwana D**, **Chow A**, **Thompson B**. Anodal transcranial direct current stimulation reduces collinear lateral inhibition in normal peripheral vision. *PLoS One* 15: e0232276, 2020.

Rideaux R, **Welchman AE**. Proscription supports robust perceptual integration by suppression in human visual cortex. *Nat Commun* 9: 1502, 2018.

Riedel G. Glutamate receptor function in learning and memory. *Behav Brain Res* 140: 1–47, 2003.

Rissanen J. Modeling by shortest data description. *Automatica* 14: 465–471, 1978.

Rokem A, **Yoon JH**, **Ooms RE**, **Maddock RJ**, **Minzenberg MJ**, **Silver MA**. Broader Visual Orientation Tuning in Patients with Schizophrenia. *Front Hum Neurosci* 5: 1–9, 2011.

Romo R, **Hernández A**, **Zainos A**. Neuronal correlates of a perceptual decision in ventral premotor cortex. *Neuron* 41: 165–73, 2004.

Sagi D. Perceptual learning in Vision Research. *Vision Res* 51: 1552–1566, 2011.

Sanaei Nezhad F, **Anton A**, **Michou E**, **Jung J**, **Parkes LM**, **Williams SR**. Quantification of GABA, glutamate and glutamine in a single measurement at 3 T using GABA-edited MEGA-PRESS. *NMR Biomed* 31: e3847, 2018.

Schallmo M-P, **Millin R**, **Kale AM**, **Kolodny T**, **Edden RAE**, **Bernier RA**, **Murray SO**. Glutamatergic facilitation of neural responses in MT enhances motion perception in humans. *Neuroimage* 184: 925–931, 2019.

Schoups A, **Vogels R**, **Qian N**, **Orban G**. Practising orientation identification improves orientation coding in V1 neurons. *Nature* 412: 549–553, 2001.

Shadlen MN, **Newsome WT**. Neural basis of a perceptual decision in the parietal cortex (area LIP) of the rhesus monkey. *J Neurophysiol* 86: 1916–36, 2001.

Shibata K, **Sasaki Y**, **Bang JW**, **Walsh EG**, **Machizawa MG**, **Tamaki M**, **Chang L-H**, **Watanabe T**. Overlearning hyperstabilizes a skill by rapidly making neurochemical processing inhibitory-dominant. *Nat Neurosci* 20: 470–475, 2017.

Sigman M, **Pan H**, **Yang Y**, **Stern E**, **Silbersweig D**, **Gilbert CD**. Top-Down Reorganization of Activity in the Visual Pathway after Learning a Shape Identification Task. *Neuron* 46: 823–835, 2005.

Smith SM, **Beckmann CF**, **Andersson J**, **Auerbach EJ**, **Bijsterbosch J**, **Douaud G**, **Duff E**, **Feinberg DA**, **Griffanti L**, **Harms MP**, **Kelly M**, **Laumann T**, **Miller KL**, **Moeller S**, **Petersen S**, **Power J**, **Salimi-Khorshidi G**, **Snyder AZ**, **Vu AT**, **Woolrich MW**, **Xu J**, **Yacoub E**, **Uğurbil K**, **Van Essen DC**, **Glasser MF**. Resting-state fMRI in the Human Connectome Project. *Neuroimage* 80: 144–168, 2013.

Soher BJ, **Semanchuk P**, **Todd D**, **Steinberg J**, **Young K**. VeSPA: integrated applications for RF pulse design, spectral simulation and MRS data analysis. In: *Proc Int Soc Magn Reson Med*. 2011, p. 1410.

Song C, **Sandberg K**, **Andersen LM**, **Blicher JU**, **Rees G**. Human Occipital and Parietal GABA Selectively Influence Visual Perception of Orientation and Size. *J Neurosci* 37: 8929–8937, 2017.

Spiegel DP, **Byblow WD**, **Hess RF**, **Thompson B**. Anodal Transcranial Direct Current Stimulation Transiently Improves Contrast Sensitivity and Normalizes Visual Cortex Activation in Individuals With Amblyopia. *Neurorehabil Neural Repair* 27: 760–769, 2013.

Stagg CJ. Magnetic Resonance Spectroscopy as a tool to study the role of GABA in motor-cortical plasticity. *Neuroimage* 86: 19–27, 2014.

Uddin LQ. Bring the Noise: Reconceptualizing Spontaneous Neural Activity. *Trends Cogn Sci* 24: 734–746, 2020.

Vaidya CJ, **Gordon EM**. Phenotypic Variability in Resting-State Functional Connectivity: Current Status. *Brain Connect* 3: 99–120, 2013.

Valtcheva S, **Venance L**. Control of Long-Term Plasticity by Glutamate Transporters. *Front Synaptic Neurosci* 11: 1–16, 2019.

Vandekerckhove J, **Tuerlinckx F**. Fitting the ratcliff diffusion model to experimental data. *Psychon Bull Rev* 14: 1011–1026, 2007.

Vandekerckhove J, **Tuerlinckx F**. Diffusion model analysis with MATLAB: A DMAT primer. *Behav Res Methods* 40: 61–72, 2008.

van Veenendaal TM, **Backes WH**, **van Bussel FCG**, **Edden RAE**, **Puts NAJ**, **Aldenkamp AP**, **Jansen JFA**. Glutamate quantification by PRESS or MEGA-PRESS: Validation, repeatability, and concordance. *Magn Reson Imaging* 48: 107–114, 2018.

Vogels R. Mechanisms of Visual Perceptual Learning in Macaque Visual Cortex. *Top Cogn Sci* 2: 239–250, 2010.

Wang K, **Smolker HR**, **Brown MS**, **Snyder HR**, **Hankin BL**, **Banich MT**. Association of γ-aminobutyric acid and glutamate/glutamine in the lateral prefrontal cortex with patterns of intrinsic functional connectivity in adults. *Brain Struct Funct* 225: 1903–1919, 2020.

Zhang J, **Rowe JB**. Dissociable mechanisms of speed-accuracy tradeoff during visual perceptual learning are revealed by a hierarchical drift-diffusion model. *Front Neurosci* 8: 1–13, 2014.

Figure Captions

Figure 1. Behavioral task and performance: (a) Orientation identification task. Participants judged the orientation of a Gabor patch presented (45° or 135°) among Gaussian noise patterns. (b) Mean performance across participants for the pretest and training blocks. Mean drift rate (c) and threshold (d) derived from diffusion modeling (DR-TH-Ter Model) across participants for the pretest and training blocks. Error bars indicate standard error of the mean across participants. We used Bayesian information criterion (BIC) for five constructed models and selected model DR-TH-Ter with the lower BIC value (i.e. null model: 3246.22, DR model: 3267.02, DR-TH model: 3234.13, DR-TH-Ter model: 3228.73, full model: 3308.36).

Figure 2. Relationship of MRS glutamate and GABA+ to behavior: (a) MRS voxels and spectra in the early visual cortex (EV) and DLPFC. We illustrate a group MRS mask (sagittal, axial view) that covers a cortical area that is common in at least 50% of the participants' MRS voxels (red: EV, yellow: DLPFC). Sample spectra from the MRS voxels show the LCModel fit, residual and respective fits for GABA+, glutamate, glutamine, glutathione and NAA. (b) Multiple regression of EV Glu with behavior: significant negative linear relationship with DR but not TH change (max-training block minus pre-training block). (c) No significant linear relationship of EV GABA+ with behavior. (d) No significant linear relationship of DLPFC Glu with behavior. (e) No significant linear relationship of DLPFC GABA+ with behavior. Significant results are indicated by closed symbols; non-significant results by open symbols.

Figure 3. Relationship of EV-DLPFC functional connectivity to behavior and glutamate: EV-DLPFC functional connectivity (Fisher's z), as measured by rs-fMRI, shows (a) a significant negative linear relationship with DR but not TH change (multiple

regression), (b) a significant positive linear relationship with EV Glu but not EV GABA+, and (c) no significant linear relationship with DLPFC Glu or GABA+. Significant results are indicated by closed symbols; non-significant results by open symbols.

Figure 4. tDCS intervention: Mean (a) Accuracy, (b) drift rate and (c) decision threshold across participants in the Anodal and Sham groups for the pretest and max-training block. Error bars indicate standard error of the mean across participants. Open circles indicate individual participant data.

Figure 1

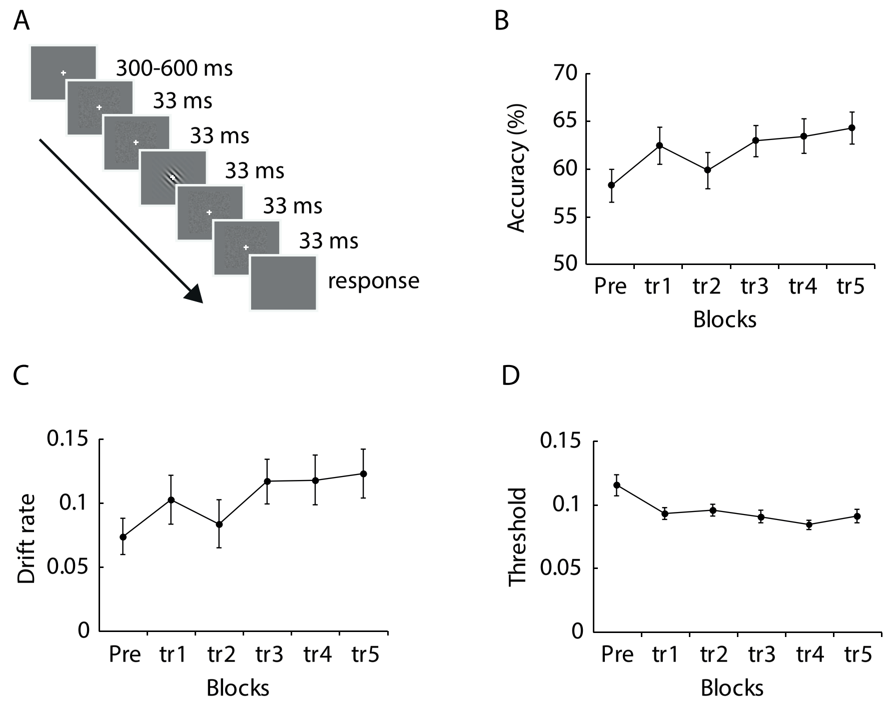
A
300-600 ms
33 ms
33 ms
33 ms
33 ms
33 ms
response
B
Accuracy (%)
70
65
60
55
50
Pre tr1 tr2 tr3 tr4 tr5
Blocks
C
Drift rate
0.15
0.1
0.05
0
Pre tr1 tr2 tr3 tr4 tr5
Blocks
D
Threshold
0.15
0.1
0.05
0
Pre tr1 tr2 tr3 tr4 tr5
Blocks

Figure 2

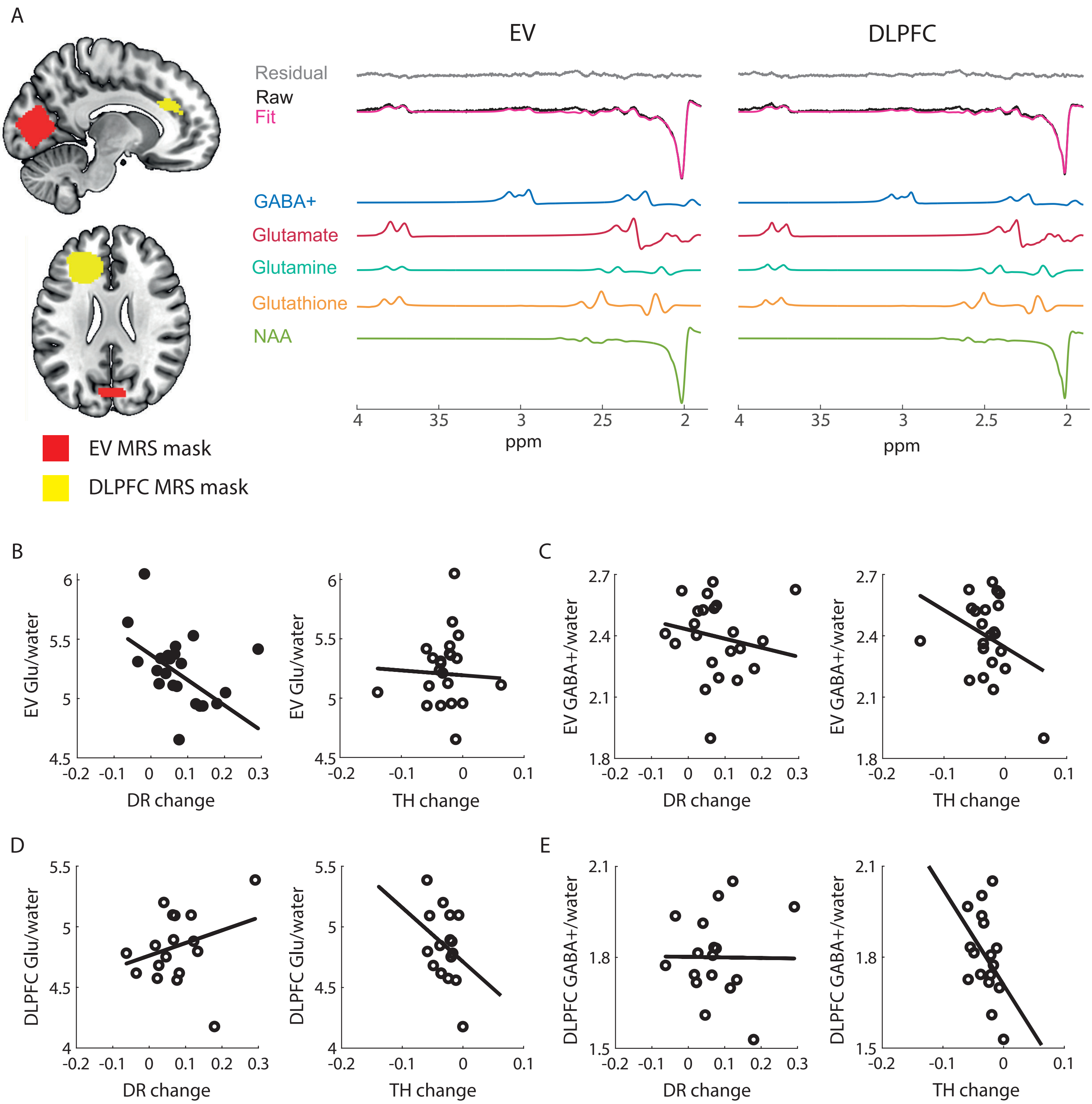

A
EV
DLPFC
Residual
Raw
Fit
GABA+
Glutamate
Glutamine
Glutathione
NAA
ppm
ppm
EV MRS mask
DLPFC MRS mask
B
EV Glu/water
DR change
TH change
C
EV GABA+/water
DR change
TH change
D
DLPFC Glu/water
DR change
TH change
E
DLPFC GABA+/water
DR change
TH change

Figure 3

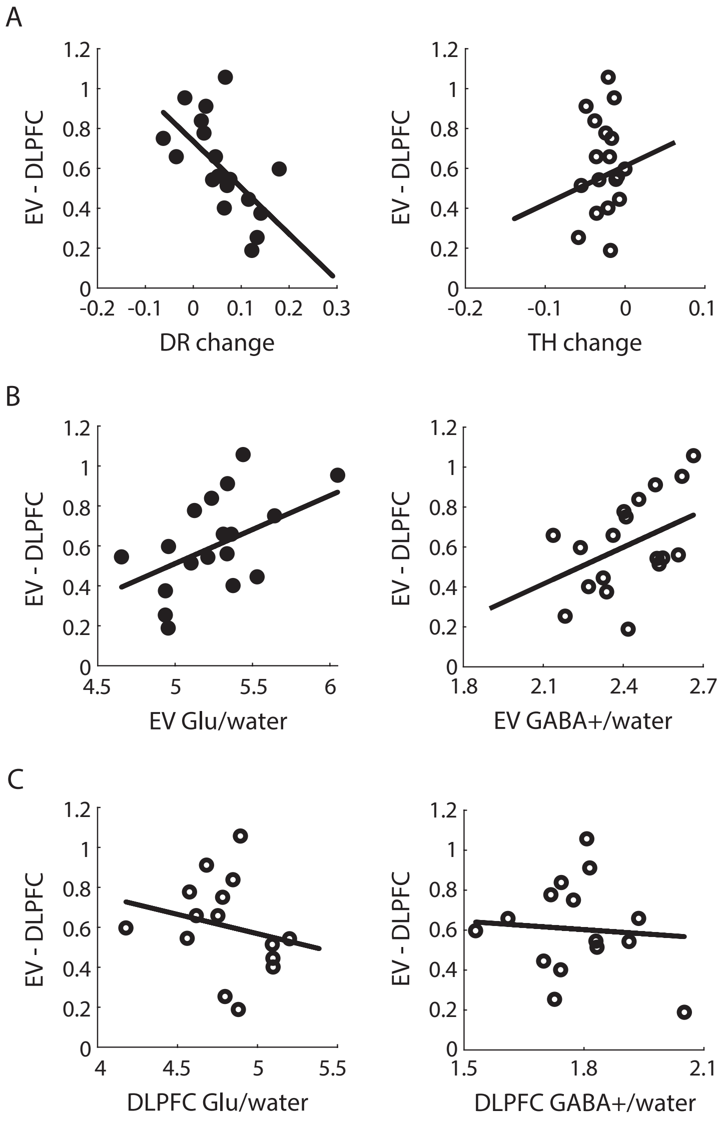
A
EV - DLPFC
DR change
TH change
B
EV Glu/water
EV GABA+/water
C
DLPFC Glu/water
DLPFC GABA+/water

Figure 4

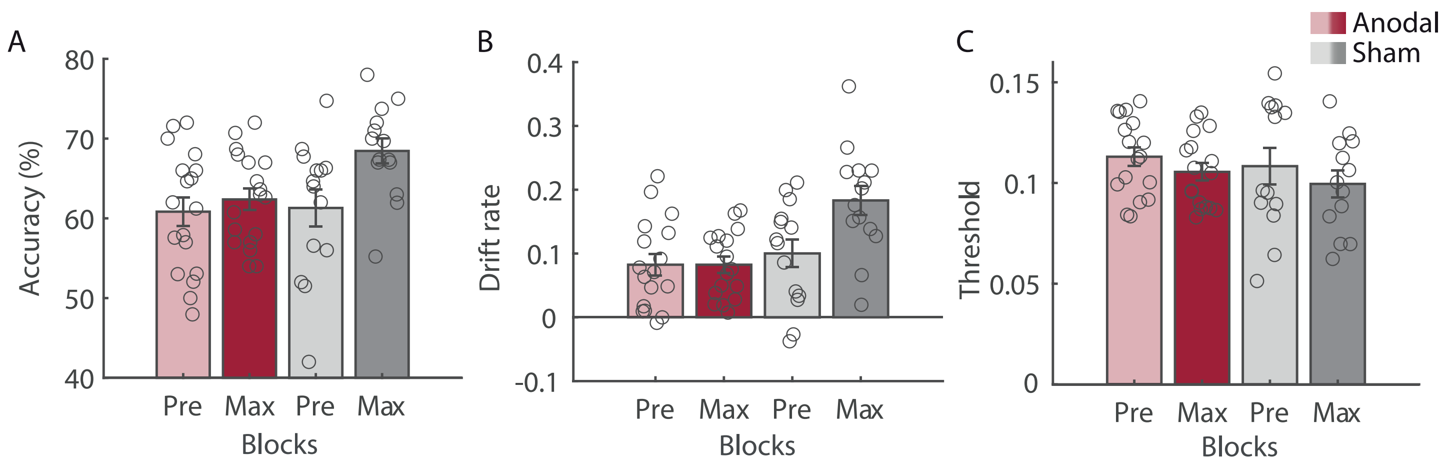
A
B
C
Accuracy (%)
80
70
60
50
40
Pre
Max
Pre
Max
Blocks
Drift rate
0.4
0.3
0.2
0.1
0
-0.1
Threshold
0.15
0.1
0.05
Anodal
Sham

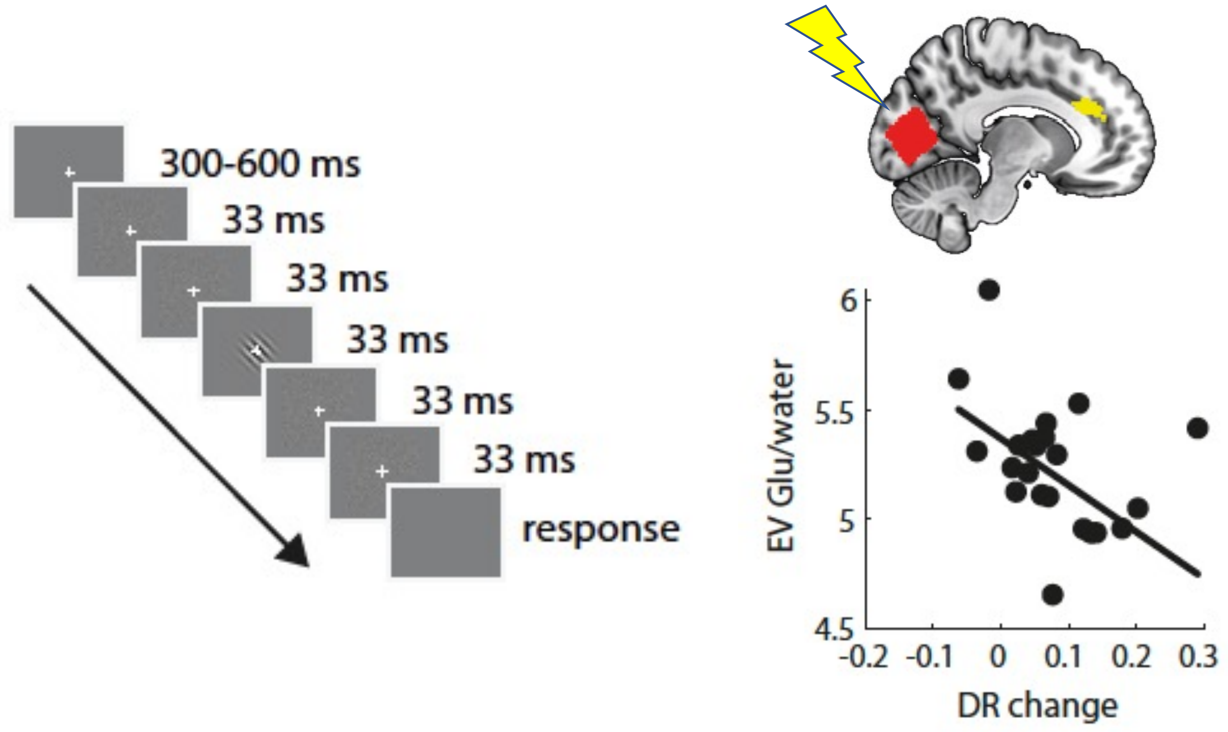

Combining multimodal brain imaging (MRS-GABA, functional connectivity) with interventions (tDCs) we demonstrate that glutamatergic excitation and functional interactions between sensory (visual) and decision-related areas (dorsolateral prefrontal cortex) support our ability to optimize perceptual decisions through training.